HHS Public Access

Author manuscript

Mol Cancer Res. Author manuscript; available in PMC 2022 October 01.

Published in final edited form as:

Mol Cancer Res. 2022 April 01; 20(4): 542–555. doi:10.1158/1541-7786.MCR-21-0275.

Integrated proteomics-based physical and functional mapping of AXL kinase signaling pathways and inhibitors define its role in cell migration

Anurima Majumder[1], **Sina Hosseinian**[1], **Mia Stroud**[1], **Emma Adhikari**[1], **James J. Saller**[2], **Matthew A. Smith**[1], **Guolin Zhang**[1], **Shruti Agarwal**[1], **Marc Creixell**[6], **Benjamin S. Meyer**[1], **Fumi Kinose**[1], **Kiah Bowers**[3], **Bin Fang**[3], **Paul A. Stewart**[4], **Eric A. Welsh**[4], **Theresa A. Boyle**[2], **Aaron S. Meyer**[6], **John M. Koomen**[5], **Eric B. Haura**[1,*]

[1]Department of Thoracic Oncology, H. Lee Moffitt Cancer Center and Research Institute, Tampa, FL 33612

[2]Department of Pathology, H. Lee Moffitt Cancer Center and Research Institute, Tampa, FL 33612

[3]Department of Proteomics and Metabolomics Core, H. Lee Moffitt Cancer Center and Research Institute, Tampa, FL 33612

[4]Department of Biostatistics and Bioinformatics Shared Resource, H. Lee Moffitt Cancer Center and Research Institute, Tampa, FL 33612

[5]Department of Molecular Oncology, H. Lee Moffitt Cancer Center and Research Institute, Tampa, FL 33612

[6]Department of Bioengineering, UCLA, Los Angeles, CA

Abstract

To better understand the signaling complexity of AXL, a member of the TAM receptor tyrosine kinase family, we created a physical and functional map of AXL signaling interactions, phosphorylation events, and target-engagement of three AXL tyrosine kinase inhibitors (TKI). We assessed AXL protein-complexes using BioID, effects of AXL TKI on global phosphoproteins using mass spectrometry, and target engagement of AXL TKI using activity-based protein profiling. BioID identifies AXL-interacting proteins that are mostly involved in cell adhesion/migration. Global phosphoproteomics show that AXL inhibition decreases phosphorylation of peptides involved in phosphatidylinositol-mediated signaling and cell adhesion/migration. Comparison of three AXL inhibitors reveals that TKI RXDX-106 inhibits pAXL, pAKT and migration/invasion of these cells without reducing their viability, while Bemcentinib exerts

[*]**To whom correspondence should be addressed:** Eric Haura, Department of Thoracic Oncology, Moffitt Cancer Center, 12902 Magnolia Drive, Tampa, FL 33612, eric.haura@moffitt.org, Tel.: 813-745-6827.

Data Availability

The supportive data for the mass spectrometry analyses have been provided as Supplemental Tables S1–S5. The mass spectrometry proteomics data have been deposited to the ProteomeXchange Consortium via the PRIDE partner repository with the dataset identifiers PXD023911 (BioID), PXD023913 (ABPP), and PXD023923 (Phosphoproteomics) (62). The Whole exome and RNA sequencing data have been deposited in SRA (PRJNA790835) and GEO (GSE191185) respectively.

Disclosure of potential conflict of interest: The authors declare no potential conflicts of interest

AXL-independent phenotypic effects on viability. Proteomic characterization of these TKIs demonstrates that they inhibit diverse targets in addition to AXL, with Bemcentinib having the most off-targets. AXL and EGFR TKI co-treatment did not reverse resistance in cell line models of Erlotinib-resistance. However, a unique vulnerability was identified in one resistant clone, wherein combination of Bemcentinib and Erlotinib inhibited cell viability and signaling. We also show that AXL is overexpressed in ~30–40% of non-small but rarely in small-cell lung cancer. Cell lines have a wide range of AXL expression, with basal activation detected rarely.

Implications: Our study defines mechanisms of action of AXL in lung cancers which can be used to establish assays to measure drug targetable active AXL-complexes in patient tissues and inform the strategy for targeting it's signaling as an anticancer therapy.

Keywords

AXL; kinase inhibitor; BioID; EGFR TKI resistance; phosphoproteomics

Introduction

Overexpression of AXL, a member of the TAM (TYRO3, AXL and MER) family of receptor tyrosine kinases, is often associated with epithelial-mesenchymal transition, increased aggressiveness, and poor prognosis in a vast number of cancers (1–3). AXL overexpression has also been linked to the development of resistance to chemo-, immune- and targeted therapy (4–10), thus making it an attractive target for therapeutic intervention.

AXL is often reported to be overexpressed, both at mRNA and protein levels, in lung adenocarcinoma (2,11,12). However, AXL is rarely reported to be genetically amplified, fused or mutated in cancers with an alteration frequency of ~3% or less in breast, lung and head and neck squamous cell carcinoma as per data from TCGA and CPTAC3 (13,14). Thereby, it is uncertain if AXL functions as a dominant oncogenic driver like other genomically altered receptor tyrosine kinases, such as mutant EGFR or ALK. In addition, the mechanism of AXL kinase activation is complex and still poorly understood. AXL is activated by its cognate ligand, Gas6 (15). However, some studies suggest that AXL-GAS6 interaction may be constitutive and functional activation of downstream signaling is achieved only when an additional interaction with phosphatidylserine (PtdSer) on apoptotic bodies exists (16,17). Recent studies have shown that AXL can act as a sensor for localized clusters of ligands wherein extracellular vesicles enriched in PtdSer accumulate Gas6 leading to an increase in local ligand concentration and activation of AXL receptor signaling (18). AXL can be also be activated in a ligand-independent manner either via clustering of overexpressed protein (19) or by heterodimerization with other receptors such as EGFR and MET (7,20,21). Also, different types of cells (such as fibroblasts and bone-marrow progenitor cells) and conditions of stress (such as hypoxia and nutrient deprivation) in the tumor microenvironment can produce GAS6 and lead to microenvironment-mediated activation of AXL in cancers (22–25).

There are multiple kinds of AXL targeting agents that are in various stages of development, including ATP-competitive small molecule inhibitors, anti-AXL monoclonal antibodies (mAbs), drug-antibody conjugates, soluble receptors, and nucleotide aptamers (26,27). Of

these, small molecule AXL TKIs form the largest group and interestingly, most of these drugs that inhibit AXL were not designed against AXL but inhibit it as an off-target. Kinase inhibitors are in general known to have a wide array of targets in addition to the one that they were designed to inhibit, thereby exhibiting a range of specific and non-specific phenotypic effects. There have been contradictory reports on whether AXL inhibition with TKIs is able to restore sensitivity to the targeted agent (28,29). This could be because the mechanism for AXL-mediated drug resistance is not well understood or because of differences in model systems and/or AXL targeting strategies used for these studies. A study on kinases capable of bypassing EGFR dependence in EGFR-mutant non-small cell lung cancer (NSCLC) cells shows that while most of the common bypass kinases were associated with sustained activation of either phospho-AKT or both phospho-AKT and ERK, AXL was associated with sustained phospho-ERK activation only, thereby suggesting that AXL had different mechanisms to rescue EGFR mutations compared to other EGFR bypass genes (30). These studies re-emphasize the importance of characterizing off-targets of purported specific kinase inhibitors as well as generating context-dependent signaling maps for AXL.

Given the complexities associated with AXL kinase activation and its context-dependency, signaling downstream of AXL is also not well defined. Small scale, focused studies in specific model systems have reported that GAS6/AXL can activate a wide array of pathways, including AKT, ERK, SRC, FAK/RAC and JAK-STAT (31,32). However, the pathways activated and hence the phenotypic response elicited by AXL signaling depends on cell/tissue type and disease state. Yet, no unbiased AXL protein complex or global phosphoproteomic analyses have been reported and it is important that such systems biology approaches be utilized to elucidate AXL's role in primary oncogenesis, metastasis and resistance to therapy.

In the current study, we aim to better characterize AXL TKIs, understand their effects on signaling and phenotype of cells, and develop assays to visualize active AXL signaling complexes. For this, we used multiple mass spectrometry-based proteomics approaches, such as proximity-dependent biotinylation (BioID) and phosphoproteomics to delineate AXL-mediated signaling in lung cancers. Our proteomic analyses provide insights into AXL interacting partners, changes in the phosphoproteome after pharmacological AXL inhibition, and putative AXL pathway substrates, which can serve as a valuable resource for understanding AXL signal activation at a systems-level. Subsequent comparative analysis of different AXL TKIs using western blotting (WB), viability assays and activity-based protein profiling (ABPP), identifies diverse target profiles and phenotypic effects for each inhibitor. In addition, treatment of our cell line models of acquired erlotinib resistance with EGFR and AXL TKI combination therapy demonstrate inability of pharmacological inhibition of AXL to reverse resistance to erlotinib in these model systems. Notably, our mass spectrometry and phenotypic assay data cumulatively show coupling of AXL to downstream PI3K/AKT signaling, but not MEK/ERK, and reveal a key role for AXL in mediating cell migration/invasion in a lung cancer cell line model. These results can guide the development of proximity ligation assays to detect active AXL signaling foci *in situ*, that can help identify patients likely to benefit from AXL targeted therapy.

Materials and Methods

Cell lines and reagents

Cells were provided by the Moffitt Lung Cancer Center of Excellence Cell Line Core. The H1299 AXL KO and PC9 AXL KO cells were developed in the Meyer lab at UCLA. Cells were confirmed to be free of mycoplasma (PlasmoTest, Invivogen) and authenticated by short tandem repeat (STR) analysis (ACTG Inc.). RXDX106, Bemcentinib and Cabozantinib were purchased from Selleckchem, dissolved in DMSO at 10 mM concentration and diluted as necessary.

Proximity-dependent biotinylation (BioID)

AXL variant 1 (from Meyer lab at UCLA) was cloned into the pENTR TOPO vector using pENTR D-TOPO cloning kit (Invitrogen) as per manufacturer's protocol. AXL was then transferred from the entry clone to pSTV6-C-BirA*-FLAG Gateway destination vector (33) (a gift from Gingras lab, Lunenfeld-Tanenbaum Research Institute) using LR-Gateway cloning, creating pSTV6-C-BirA*-FLAG-AXL lentiviral vector. Lentivirus packaging was done as described before (33). H1299 cells were infected with the produced virus and then supplemented with 2 μg/ml puromycin for selection 48 hours post-transfection to generate H1299 cells stably expressing pSTV6-C-BirA*-FLAG-AXL.

Cells were grown and expanded into one 15 cm petri dish per replicate for BioID proteomics experiments. Three biological replicates were used per sample. Samples for BioID proteomics analysis were prepared using methods described in (33). LC-MS/MS was carried out on the Thermo Q Exactive Plus quadrupole-orbitrap hybrid mass spectrometer. Peptides identified using Proteome Discoverer (2.2.0.388) and visualized using Scaffold (4.8.7). Putative AXL binding partners were identified by Automated Processing of SAINT Templated Layouts (APOSTL) (34).

Proximity Ligation Assays

Proximity Ligation Assays (PLA) were performed as described (35). Briefly, cells were plated, fixed and permeabilized in eight-well chamber slides. Non-specific binding was blocked, followed by overnight incubation at 4°C with primary antibodies, rabbit anti-AXL (Cell Signaling 8661) and mouse anti-pY (pY-100; Cell Signaling 9411). Subsequent incubations with rabbit (+) and mouse (–) PLA probes and detection with Duolink In Situ Detection Reagents FarRed (Sigma) were carried out as per the manufacturer's protocol. Fluorescent images were acquired on a fully automated upright Zeiss Axio Imager Z.1 microscope at 40X magnification using Axiovision software suite (version 4.6, Carl Zeiss Inc.).

Phosphoproteomics

H1299 cells were plated in six 15cm dishes for each sample (in triplicates) and treated with RXDX-106. Phosphoproteomics samples were prepared using the PTMScan Kit (Cell Signaling) as per the manufacturer's protocol. Phosphotyrosine peptides were enriched using the antibody beads (PTMScan Phospho-Tyrosine Rabbit mAb (P-Tyr-1000) Kit, Cell Signaling #8803) and analyzed with LC-MS/MS for label-free quantitation.

The flow through from the immunoprecipitation of phosphotyrosine peptides was labeled using TMT 10-plex reagents following the manufacturer's recommendation (TMT10plex™ Isobaric Label Reagent Set, Thermo Fisher Scientific), enriched using IMAC and used for global phosphoproteomics (pSTY).

A nanoflow ultra-HPLC (RSLCnano, Thermo, Sunnyvale, CA) coupled to a quadrupole-orbitrap hybrid mass spectrometer (Q Exactive Plus, Thermo, San Jose, CA) was used for LC-MS/MS analysis. MaxQuant 1.5.2.8 (36) was used for peptide identification and reporter ion quantification. Data were normalized and analyzed for differential expression between different treatment conditions.

Scratch wound cell migration and invasion assays

Scratch wound cell migration and invasion assays were carried out per the recommended protocol for the IncuCyte system (Essen Bioscience).

Activity-Based Protein Profiling (ABPP)

H1299 and PC9 cell pellets, in triplicate for each sample, were harvested in ice-cold PBS, lysed, and the ATP-binding proteome labeled according to the Pierce Kinase Enrichment Kits and ActivX™ Probes (Thermo Scientific, Rockford, IL, USA). Lysates were incubated with 20 μM RXDX106, Cabozantinib, Bemcentinib or DMSO for 15 minutes and the desthiobiotin-ATP probe was added for the competition reaction at a final concentration of 5 μM for 15 minutes, followed by reduction, alkylation, trypsin digestion and pulldown of desthiobiotinylated peptides. LC-MS/MS data were acquired, and peptides identified using MaxQuant. Data were normalized and analyzed for differential expression between different drug treatments.

Generation of Resistant Cell Lines

Cell lines models for acquired resistance to first-generation EGFR TKI, erlotinib, were derived by dose escalation treatment of EGFR-mutant cell lines with erlotinib as described before (37). The cell line models for perister-derived erlotinib resistance were generated by passing PC9 cells through a persister bottleneck as described before (38). Briefly, parental PC9 cells were exposed to 2.5 μM erlotinib for ~6 weeks until few surviving single cells were observed. After passing through a senescent period, single cells emerged to form colonies. These colonies were isolated, passaged to new plates, and maintained in 1 μM erlotinib for further studies.

DNA/RNA sequencing

DNA and RNA were extracted simultaneously using QIAGEN AllPrep DNA/RNA mini kit as per manufacturer's protocol. From extracted RNA, RNA-sequencing libraries were prepared using the NuGen FFPE RNA-Seq Multiplex System (Tecan US, Inc., Morrisville, NC). Whole-exome sequencing was performed on extracted genomic DNA using the Agilent SureSelect XT Clinical Research Exome kit (Agilent Technologies, Inc., Wilmington DE).

Gene expression data were normalized and differential expression between experimental groups were evaluated using DEseq2 (39). RNA sequencing data were filtered, and

normalized genes were subjected to single sample gene set enrichment analysis (ssGSEA) using the cancer hallmarks (40). The ssGSEA parameters used were sample.norm.type: rank, weight: 0.75, statistic: area.under.RES, output.score.type NES, nperm: 1000, min.overlap: 5, correl.type: z.score, and run.parallel: TRUE. ssGSEA results were visualized using the Complex Heatmap R package (41). Gene sets with FDR > 0.05 were denoted with an "X".

For detailed experimental procedures, see the Supplementary Materials and Methods.

Results

Proximity-dependent biotinylation identifies AXL interacting proteins that are mostly involved in cell adhesion/migration signaling

We took an unbiased multipronged systems level proteomics approach, consisting of proximity-dependent biotinylation (BioID) interaction mapping as well as tyrosine and global phosphoproteomics, to annotate AXL protein complexes and investigate AXL signaling in lung cancers (Figure 1A). We hypothesize that the identified interacting and signaling proteins and their functions would guide the understanding of AXL's role in these cells. For this, H1299 NSCLC cells were chosen as they are known to have high levels of AXL expression and activation and are more likely to give us pertinent interacting proteins and mechanisms. To identify AXL interacting proteins, we used the BioID system which utilizes a proximity-dependent labeling strategy. For this, the bait protein is fused to a mutant form of biotin ligase (BirA*) that biotinylates interacting protein within a 10 nm radius of the protein of interest, which can then be enriched and identified by mass spectrometry (33). This system allows for harsher lysis conditions over other affinity-based mass spectrometry approaches because proximal proteins are now marked by covalent biotin modifications and preservation of protein complexes is not necessary for identification.

H1299 cells expressing pSTV6-BirA*-FLAG-AXL were created. To confirm expression of the transgene, immunofluorescence staining with anti-FLAG antibody was done on parental H1299 and induced H1299-BirA*-FLAG-AXL cells. FLAG staining, with distinct membrane localization, was observed only in the cells that were transduced with the transgene and induced with doxycycline and biotin (Figure 1B). H1299-BirA*-FLAG-AXL-Puro cells were then either treated with biotin only (negative control, no expression of BirA*-FLAG-AXL), doxycycline only (negative control, BirA*-FLAG-AXL expressed but no biotinylation), and both biotin and doxycycline (expression and biotinylation of BirA*-FLAG-AXL). Treated cells were lysed, processed and prepared for mass spectrometry analysis (Figure 1A). The data was then analyzed using APOSTL (34) wherein the proteins found in the negative controls were subtracted to identify 119 AXL interacting proteins. The results show that the biotinylated bait protein, AXL, was only detected in the sample that was induced with both biotin and doxycycline, as expected (Figure 1C). Other proteins identified as putative AXL interactors included known partner proteins, such as EGFR and ITGB1, as well other interesting proteins known to be involved in kinase biology (such as ERBB2IP, GAB1, STAT3, PTPN11 and SCRIB) (Figure 1C). To identify signaling pathways and functional modules that are associated with the AXL interactome, these proteins were further subject to STRING-based network and KEGG and GO-based pathway analyses. STRING network analysis with high confidence resulted in an undirected network with 119

nodes (proteins) and 150 edges (interactions) that was imported and visualized in Cytoscape (Figure 1C). The AXL interacting proteins could be classified into adherens/tight junction (consisting of ITGB1, BAIAP2, YES1, LLG1, EGFR, EZR, SCRIB, CTNND1, TJP1, DLG1, MLLT4, OCLN, PVRL2), cell junction assembly/organization (consisting of CTTN, FERMT2, ITGA2, ITGA6, GJC1, DSG2, NUMBL, FLNA, NUMB, PVRL2, OCLN, MLLT4, DLG1, TJP1, CTNND1) and protein localization to cell periphery (consisting of EPB41L2, ITGB1, EGFR, DLG1, EZR, SCRIB, NUMB, FLNA, PALM, VAMP3, CAV1, EPHA2, PICALM, FLOT1) clusters (Figure 1C). We identified adherens/tight junction, proteoglycans in cancer, cell junction assembly/organization and protein localization to the cell periphery as the top enriched functional modules from KEGG and GO analyses (Figure 1C and D), thereby suggesting that AXL has a major role to play in regulating cell adhesion and migration in these cells.

Pharmacological AXL inhibition deregulates phosphorylation of peptides in downstream phosphatidylinositol mediated signaling and cell adhesion/migration pathway

In addition to profiling AXL interactors by BioID, we performed tyrosine (pY) and global (pSTY) phosphoproteomics in H1299 cells treated with an AXL kinase inhibitor to understand signaling downstream of AXL kinase activation. For this, a potent TAM inhibitor, RXDX106, was used. We first treated H1299 cells with RXDX106 for varying amounts of time to confirm its ability to inhibit AXL phosphorylation by western blotting (Figure 2A). Our data shows that 100 nM of RXDX106 potently inhibited AXL phosphorylation at Tyr^{702} within 30 min. This was accompanied by a concurrent increase in AXL and a decrease in phosphorylation of downstream AKT (both at Ser^{473} and Thr^{308}), but not ERK (Figure 2A). We also show that siRNA mediated silencing of AXL expression triggers a decrease in downstream pAKT without altering the pERK levels (Figure 2A). This suggests that AXL activation is driving downstream PI3 kinase/AKT signaling events in this model. As an alternate method to assess changes in AXL tyrosine phosphorylation and activation, that can potentially to be translated to clinic as a diagnostic platform, we developed Proximity Ligation Assays (PLA) to detect activated AXL:pY signaling complexes in these cells. H1299 and Calu1 cells, both of which have detectable levels of phosphorylated AXL Tyr^{702} (Figure 6C), have high basal AXL:pY PLA foci that are abrogated by treatment with AXL TKI, RXDX106 (Figure 2B). As expected, the HCC827 cells, which lack pAXL, do not show significant labeling in this PLA (Figure 2B).

For the phosphoproteomics profiling, we treated H1299 cells either with DMSO or RXDX106 for 0.5 or 4 hours. Cells were then lysed, trypsin digested and processed for mass spectrometry (Figure 1A). In the global phosphoproteomics dataset, we identified 13638 unique phosphopeptides, which correspond to 3679 unique phosphoproteins. In the pY dataset, 634 unique phosphopeptides, corresponding to 329 unique phosphoproteins, were identified. We focused on the phosphopeptides that are significantly altered by AXL inhibitor, RXDX106. A phosphopeptide was determined to be differentially expressed (DE) between two conditions if $|\log_2 \text{ratio}| \geq \sim 0.585$ (1.5-fold change) and p-value < 0.05. This filtering analysis gave us 148 unique peptides (mapped to 105 unique proteins) from the pY dataset and 5117 unique peptides (mapped to 2032 unique proteins) from the pSTY dataset.

To gain a global view of signaling networks regulated by AXL kinase, we generated an experimentally consistent literature network. For this, DE phosphopeptides from the pSTY and pY datasets were combined and assigned to five broad pattern categories as shown in Figure S1A. Selected DE phosphoproteins were then searched for activating or inhibiting transcriptional and phosphorylation literature interactions with MetaCore followed by in-house filtering for experimental consistency and visualization to generate the network shown in Figure S1A.

This experimentally consistent literature network provides a global view of the signaling networks regulated by AXL. As expected, phosphorylation of TAM kinases, including AXL, were downregulated as they are known targets of RXDX106 (42). The network shows decreased phosphorylation of several proteins, including kinases such as PAK2 and PAK4 and other proteins such as CTTN, KRT18, NUMB, that are involved in cell adhesion, migration and actin reorganization. Protein kinases, such as ERBB2, CDK2, MTOR, PRKCD and several MAPKs (MAPK1, 3, 7), had increased phosphorylation as per the network. Increased MYC, ETS1, and JUN phosphorylation were also shown as prominent nodes with high connectivity (Figure S1A).

We identified signaling by Rho GTPases, which are known to regulate cytoskeletal and cell adhesion dynamics, as the top enriched pathway from MsigDB (40) canonical pathways (CP) analysis (Figure S1A).

We also took a more focused look at the changes in only tyrosine phosphorylation induced by RXDX106 (Figure 2C). This analysis revealed affected pY sites from proteins with diverse functions and revealed both known and novel interactors of AXL. Tyrosine phosphorylation of proteins involved in cell adhesion/migration/invasion (such as TJP1, CTNND1), actin remodeling (such as CTTN, EPB41), phosphoinositide signaling (such as INPPL1, GAB1, GAB2), GTP-mediated signaling (such as RASA1, RIN1, ARHGAP35), as well as kinases (such as IGF1R, EGFR, EPHB4, LYN, FER, MAPK1/3), receptors (such as ITGB1/4), adaptor (such as LAT2, CRKL, SHB, GAB1/2, ERBIN) and scaffold (such as FLOT1) proteins, are modulated by AXL inhibition, indicating that these cellular processes may be important for propagating AXL signaling and function downstream (Figure 2C). Anchoring junction and signaling by receptor tyrosine kinases were identified as top enriched functional modules from MsigDB gene ontology (GO) and canonical pathways (CP) analyses, respectively (Figure S1B).

To identify new putative substrates of the AXL signaling pathway, we integrated the phosphoproteomics data with the proximity network. We found 23 peptides from the pY dataset that overlapped with the BioID data and used their peptide sequences to build a Position-Specific-Scoring-Matrix (PSSM) motif (Figure 3D). Transition matrices such as PAM20 are frequently used to calculate the similarity between two given sequences (43). Thereby, we computed the mean PAM250 similarity scores between each peptide sequence of the global phosphoproteomics data set and the 23 sequences forming the AXL pathway motif to rank all peptides by its similarity to the AXL pathway motif. This analysis identifies CBL, DCBLD2, LAMTOR1, ARHGAP35, LAT2, RASA1, ABI1, RIN1 and PTK2 as some of the top putative AXL pathway substrates (Figure 2D).

Overall, our data supports our earlier observation that AXL inhibition deregulates phosphorylation of proteins involved in PI3K/AKT pathway and suggests that AXL has an important role to play in cell migration signaling pathways in these cells.

AXL inhibition suppresses migration and invasion of cells but not their viability

To functionally validate the effect of AXL inhibition on the migration and viability of cells, we performed scratch wound cell migration and invasion assays as well as cell viability assays. H1299 and Calu1 NSCLC cells were treated either with DMSO, the indicated concentrations of RXDX106, or AXL siRNA. The movement/migration of cells into the scratch wound was monitored by imaging the scratch wound every three hours using the IncuCyte system until the wound was completely closed. Our data shows that inhibition of AXL with RXDX106 or siRNA reduced the wound closure rate, as measured by relative wound density, in a dose-dependent manner in both H1299 and Calu1 cells (Figure 2E, F). This implies that cells are moving into the wound slower in the presence of an AXL inhibitor or siRNA, both in migration (where the scratch is not overlaid with Matrigel, Figure 2E) as well as in invasion (where the cells are moving through the Matrigel laid over the scratch, Figure 2F) assays, thereby supporting the effect of AXL inhibition on components of the cell adhesion/migration/invasion pathways seen in our phosphoproteomics data. To assess the effect of AXL inhibition on cell viability, H1299, Calu1, H2009, H460 and HCC827 cells, each of whom express varying levels of phosphorylated and total AXL, were treated with increasing doses of RXDX106 for 72h. We observed that 1 μM RXDX106 reduced the viability of these cells only by ~10%, except for H2009 whose viability was reduced by ~ 50% (Figure 2G). Reduction of viability of cells was only observed at high doses of 5 and 10 μM RXDX106 in all cell lines studied, irrespective of their level of AXL expression. Interestingly, for H1299 and Calu1, cell viability was not altered at drug doses of 100 nM or 1 μM (Figure 2G) that were shown to inhibit phosphorylation of AXL (Figure 2A, B) and migration/invasion of cells (Figure 2E, F). Collectively, these data provide a map for AXL protein-complexes and signaling partners and evidence for AXL's role in mediating cell migration/invasion.

AXL kinase inhibitor, Bemcentinib, exhibits AXL-independent phenotypic effects

In our data, doses of AXL inhibitor RXDX106 that reduced AXL phosphorylation did not significantly alter viability of the lung cancer cells tested. However, there are reports in literature of other AXL inhibitors that reduce cell viability as well as reports of divergent effects of different AXL TKIs on cell viability (28,44). These discrepancies could be attributed to the polypharmacology effect of kinase inhibitors wherein these drugs display a wide spectrum of targets in addition to the specific target they were designed against (45). To understand the differences in phenotypic effects between different AXL inhibitors, we compared three AXL inhibitors, RXDX-106 (a TAM inhibitor (42)), Cabozantinib (a multikinase inhibitor that inhibits AXL (46)) and Bemcentinib (an AXL inhibitor currently in clinical trials (47)) in short-term viability assays, long-term colony formation assays, as well as their ability to modulate signaling downstream of AXL (Figure 3). For these studies, along with H1299 cells, EGFR mutation driven PC9 NSCLC cells were also used, since we were interested in subsequently looking at the role of AXL in the context of ERFR TKI resistance. To differentiate AXL-dependent effects from AXL-independent ones, we also

used H1299 and PC9 cells where AXL has been knocked out by CRISPR (AXL KO) in these studies. In addition to AXL inhibitors, PC9 cells were also treated with Erlotinib as a control drug, since its ability to potently inhibit viability, colony-formation and signaling in EGFR-mutant PC9 cells is well characterized. We observe that Bemcentinib is more effective in reducing the viability of cells compared to other AXL inhibitors in both H1299 (Figure 3 A, B) and PC9 cells (Figure 3 F, G). This difference is more evident in the colony-forming assay, where 1 μM Bemcentinib completely inhibits growth in both H1299 and PC9 cells. Interestingly, Bemcentinib shows more robust decrease in cell viability and colony forming assays than the other AXL inhibitors even in H1299 and PC9 AXL KO cells (Figure 3D, E, I, J), thereby suggesting that this effect on viability of Bemcentinib is likely AXL-independent. The effect of each of these AXL inhibitors on downstream signaling was also assessed by treating H1299 and PC9 cells with the indicated concentration of drugs for an hour (Figure 3C, H). RXDX106 and Cabozantinib both reduced AXL phosphorylation at Tyr^{702} concomitant with a reduction in downstream AKT phosphorylation in H1299 cells. Bemcentinib was observed to cause a decrease in downstream AKT phosphorylation without inducing a robust inhibition of AXL $pTyr^{702}$ (Figure 3C), which is consistent with previous reports of Bemcentinib inhibiting AXL phosphorylation at tyrosine residues other than Y702 (47). In PC9 cells that express AXL but not detectable pAXL, RXDX106 and Cabozantinib do not alter downstream pAKT or pERK (Figure 3H). Interestingly, treatment with Bencentinib decreases pAKT and completely inhibits pERK in PC9 as well as PC9 AXL KO cells at 1 μM, thereby suggesting that this effect on signaling is AXL-independent (Figure 3H, K). Treatment with Erlotinib inhibits pEGFR Tyr^{1068}, pAKT and pERK as expected in EGFR-driven PC9 cells (Figure 3H).

To compare the kinase-binding targets between these three AXL inhibitors that exhibit diverse phenotypic and signaling responses, we performed an activity-based protein profiling (ABPP) experiment in both H1299 and PC9 cells as shown in Figure 4A. ATP-ABPP is a chemical proteomic tool that uses a kinase active-site directed competitive ATP probe to enrich and identify kinase binding targets and off-targets of a drug based on its activity (48,49). Identified proteins from the ABPP experiment were labeled to be differentially expressed (DE) between conditions using 1.5-fold and $p < 0.05$ cutoffs. Kinases were our primary focus, so we filtered the differentially expressed proteins to select for protein kinases that were present in the DMSO control sample but significantly reduced in the drug treated samples. Kinases that were present in all DMSO samples but absent in all drug-treated samples, were manually selected to be DE since statistics could not be derived for these proteins. We observed that each drug had a unique kinase binding profile as illustrated in the kinome trees (Figure 4B, E). Despite this heterogeneity, ten and eight kinases, including AXL, were common targets of all 3 drugs in H1299 and PC9 cells respectively (Figure 4B, D, E, G). Interestingly, there is a high degree of concordance between the kinase targets of a drug in the two different cell lines tested, with ~60% of the kinases being similar for Bemcentinib and RXDX106 and ~65% for Cabozantinib (Figure 4C, F). Our data also showed that Bemcentinib binds more kinases compared to the other two AXL inhibitors, thereby resulting in perturbations of the ATP-binding proteome that were distinctly different (Figure 4 B, C, E, F). Proteins altered uniquely by Bemcentinib belonged to the CK1, AGC and CAMK kinase families (Figure 4B, E) and when subjected

to pathway enrichment analysis using ENRICHR (50), the topmost enriched pathway was found to be MAPK signaling.

Overall, here we compare the phenotypic and signaling effects of three commonly used AXL inhibitors and identify the spectrum of kinase targets for each of them. Our data suggests that of the three AXL TKIs characterized here, Bemcentinib has the most off-targets and that viability effects of Bemcentinib do not require AXL. The promiscuity of Bemcentinib may help explain the unique phenotypic and signaling perturbations induced by this drug, including its AXL-independent effects.

AXL and EGFR TKI combination treatment does not reverse EGFR TKI resistance in cell-line models of Erlotinib-resistance

Given the recent reports on the role of AXL in mediating resistance to EGFR-targeted therapy (7,8,10), we used two types of cell line models of Erlotinib-resistance to investigate the effect of AXL inhibitors on EGFR TKI resistance. For our first model, EGFR-mutant PC9 cells were passed through a persister bottleneck (38) by applying strong drug selection pressure to generate drug-tolerant erlotinib persister cells. We created four Erlotinib-resistant clones from one parental population; S1–34, S2–10, S2–17 and S2–30. We found AXL to be overexpressed in each of these clones (Figure 5B). To investigate the role of AXL in acquired resistance in persister-derived erlotinib-resistant cells, we treated PC9 and each of the clones either with Erlotinib, RXDX106 or Bemcentinib alone or in combination and assessed for changes in cell viability and signaling events (Figure 5 A, B). Erlotinib inhibited PC9 cell viability and induced complete shutdown of EGFR, AKT and ERK signaling, as expected. AXL inhibitors, RXDX106 and Bemcentinib, on the other hand had minimal effect on PC9 cell viability by themselves. Interestingly, while RXDX106 had no effect on EGFR and its downstream signaling, Bemcentinib showed inhibition of ERK phosphorylation without altering EGFR or AKT phosphorylation (Figure 5A, B). The unique effect of Bemcentinib on ERK phosphorylation could be due to the MAPK targets of this drug that we identified via ABPP. These persister-derived cells were all uniformly resistant to Erlotinib as well as AXL inhibitors as single agents, but had diverse responses in corresponding EGFR, AKT and ERK activity downregulation. Combination of EGFR and AXL TKIs were in general ineffective in reversing Erlotinib resistance in these cells, except for the unique effect of Bemcentinib and Erlotinib co-treatment in S2–10. S2–10 is resistant to Erlotinib and Bemcentinib as single agents, but when exposed to the combination, this clone showed inhibition of EGFR and ERK activity and a reduction in cell viability that the other persister-derived resistant cells did not show. The other AXL inhibitor, RXDX106, did not exhibit this combination effect in any of the resistant cells (Figure 5A, B).

Whole exome and RNA sequencing analyses were performed to probe the differences in Erlotinib-resistance mechanisms present in these persister-derived Erlotinib-resistant cells. Overall, our whole exome and RNA sequencing data reveals the heterogeneity of the clones that emerged from the persister bottle neck (Figure S2, S3). From the whole exome sequencing data that identified genetic changes between parental PC9 and each of the resistant cells, we first looked for mechanisms of erlotinib resistance commonly reported in clinical studies. EGFR T790M mutation allele frequency for each

of the clones and their corresponding sensitivity to Osimertinib are shown in Figure 5E. Mutations in the other commonly implicated pathways, such as MET, MAPK, PI3K, were not detected in our resistant clones. We filtered DNA mutations based on their PolyPhen-2 score, a tool used to characterize mutations as “possibly damaging” and “probably damaging.” Figure S2 and Table S6 shows the whole spectrum of probably damaging variants which are present in any of the resistant clones compared to the parental PC9 cells. Our data reveals 57 variants that were uniquely present or absent in one clone (for instance, IBTK mutation was only present in S2–10 while OTUD7A and ARAP2 were mutated only in S2–30). We also found 10 variants that were either gained or lost across all resistant cells compared to PC9 (like MAP7D1, RGS7BP, C7orf26 etc). mRNA analysis focused on the “hallmarks” of cancer were plotted as a heatmap to show changes in each of the clones compared to parental PC9 cells (Figure S3). Some hallmarks, such as WNT_BETA_CATENIN, REACTIVE_OXYGEN_SPECIES and TGF_BETA_SIGNALING, were found to be commonly up-regulated in all resistant cells while others, such as OXIDATIVE_PHOSPHORYLATION, E2F_TARGETS, and NOTCH_SIGNALING, were down-regulated in all of the clones. The expression of different EMT-related genes derived from the RNA sequencing data is shown in Figure 5E and shows diverse profiles of these markers amongst the different resistant clones. Consistent with our previous data (Figure 5B), the only gene found to be upregulated in all four persister-derived resistant cells was AXL.

For our second model, two EGFR-mutation–driven NSCLC cells (HCC4006 and HCC827) were exposed over time to increasing doses of erlotinib, a first-generation EGFR TKI, to generate HCC4006ER and HCC827ER cells that did not acquire EGFR T790M mutation and exhibited erlotinib resistance and EMT features (37). The HCC827ER cells generated did not have MET amplification. Both these resistant cell lines were found to overexpress AXL compared to the parental cells (Figure 5C). These cells were then treated either with erlotinib, RXDX106 or Bemcentinib alone or in combination and assessed for changes in cell viability and signaling events (Figure 5C, D)). As expected, the HCC4006 and HCC827 parental cells are sensitive to Erlotinib, whereas the HCC4006ER and HCC827ER cells are resistant (Figure 5D). Erlotinib treatment completely inhibited EGFR Tyr^{1068} phosphorylation in both parental and ER cells. Downstream AKT and ERK activity was concurrently inhibited in the parental cells whereas this activity was retained in the ER cells (Figure 5C), thereby leading to drug resistance. The AXL inhibitors, alone or in combination with Erlotinib, were unable to increase inhibition of AKT and ERK or reverse Erlotinib resistance in the ER cells (Figure 5C, D).

Our data also shows that EGFR and AXL TKI combination treatment fails to reverse resistance in two different cell line models of erlotinib resistance, except for the unique effect of Bemcentinib on one persister-derived Erlotinib-resistant cell, where it re-sensitizes the resistant cell to Erlotinib in an AXL-independent manner. The heterogeneity among the various persister-derived Erlotinib-resistant cells is probably an underlying mediator of the differential effects observed.

Landscape of AXL expression in lung cancers

Studies surveying AXL expression in human lung cancer patient samples have reported a wide range of AXL overexpression levels, ranging from 33% - 93%, possibly due to differences in antibodies and staining methods used (32). The varying sub-types, stage and histology of the patient samples as well as the size of the cohort studied may also contribute to the differing numbers from each report. The largest study on AXL expression in clinical samples so far consists of 134 NSCLC tumors (51). For more comprehensive view of the landscape of AXL expression in lung cancer patients, we used AXL immunohistochemistry to screen patient tumor microarrays (TMAs), consisting of more than 500 tissue samples from small-cell, squamous-cell and adeno carcinomas, to assess the overall expression of AXL protein in lung cancers. A score of 0–3 was assigned to each tissue section based on staining intensity (Figure 6A). Our data shows that AXL expression is high in ~30–40% of NSCLC patients, irrespective of their histology or mutational status (Figure 6B). High AXL expression was detected in 27.8% of the squamous sample and 38.5% of the adenocarcinoma samples. There is however very low prevalence of AXL overexpression in SCLC patient tissues with only ~8% of the samples having high AXL staining (Figure 6B). Prevalence of AXL positivity was not affected by driver mutation status with 42.5% of the EGFR mutant, 41.2% of the KRAS mutant, and 40.9% of the ALK-positive tissue samples having high AXL expression by immunohistochemistry (Figure 6B). Interestingly, significant fraction of KRAS mutant cancers having high AXL can have implication for KRAS therapeutics in development as recent data suggests that AXL can be a bypass signaling mechanism in KRAS G12C inhibitor treated cells (52). Twenty lung cancer cell lines were also screened for AXL protein expression using western blotting and we found a wide range of AXL expression across these lines (Figure 6C). Most (~ 75%) of the cell lines screened had some level of AXL protein expression. Interestingly, AXL was detected to be endogenously activated by phosphorylation at Tyr^{702} only in 3 of the 20 cell lines screened (H1299, Calu1, H2009), with H1299 having the highest levels of phosphorylated AXL (Figure 6C). The comprehensive data from this large set of TMAs and cohort of cell lines provides a view of the landscape of AXL expression across lung cancer tumor tissues and cell line models.

Discussion

In this study, we utilize multiple system-wide proteomic approaches to identify AXL-associated interacting partners and signaling networks, and drug target profiles for AXL TKIs used as probes and in clinics for lung cancers. To our knowledge, this is the first study to use multiple proteomics approaches to probe the AXL interactome, phosphoproteome, and response to pharmacologic AXL inhibition at a systems level. This study will aid in improving our understanding of AXL-dependent signaling as there is limited information available about this. In fact, a search of BioGRID, a curated interaction repository, for known AXL interactors yields a list of only 70 unique interactors, as compared to a list of 1293 unique interactors for EGFR, clearly demonstrating the gap in knowledge about AXL-driven signaling. Most of these previously reported AXL interactors were identified from low-throughput assays and the ones identified via high-throughput screening were not from studies designed to investigate AXL biology. Our data from AXL protein complex

annotation by BioID identified 118 novel AXL interacting proteins and reveal a primary role for AXL in mediating cell adhesion/invasion and identify several proteins involved in this process downstream of AXL. Several groups have reported over-expression of AXL associated with EMT, cell migration/invasion and cancer metastasis (11,12,53,54), but specific protein partners coupled to AXL that are involved in this were not identified.

Our global phosphoproteomics and supporting western blotting data shows coupling of AXL predominantly to downstream PI3K/AKT and not MAPK signaling in H1299 cells. Other groups have observed AXL-dependent activation of MEK/ERK signaling (55–57), possibly due to the chimeric receptors and/or the model systems used in these studies. Moreover, we found that inhibition of AXL signaling does not affect viability of cells that have high AXL activation at doses sufficient to block AXL activity. Our self-consistent map of the phosphoproteomics data show upregulation of phosphorylation in nodes such as ERBB2, CDK2, several MAPKs (MAPK1, 3, 7), MYC, ETS1, and JUN, which are known to be involved in prosurvival signaling, and could explain adaptive mechanisms that help these cells evade death from AXL inhibition. These observations highlight a limitation in studying AXL's mechanism of activation and action, which is the lack of an ideal *in vitro* model system. AXL is rarely reported to be genetically altered and hence AXL-driven cell line models of cancers are lacking. Cell lines that we and others and have used to study AXL signaling are driven by other dominant drivers and have concomitant overexpression of AXL, such as the NRAS mutation driving H1299 cells. As such AXL functions as a co/secondary driver in these models. Data derived from such models are complicated by the presence of these dominant background mutations making it challenging to delineate effects controlled by AXL versus the ones exerted by the background mutation.

Several AXL targeting agents are in various stages of preclinical development and more are advancing into different stages of clinical investigation (27). The majority of these AXL inhibitors are actually multi-kinase inhibitors (27) whose target profiles and mode of action have not been fully elucidated. As they are given to patients, this information will help predict and circumvent possible side-effects and future resistance mechanisms. Here, we used activity-based protein profiling to identify and compare the target binding profile of three AXL inhibitors, a TAM inhibitor RXDX106, an FDA approved multikinase inhibitor Cabozantinib, and an AXL inhibitor Bemcentinib being evaluated in clinical trials. Our data shows diverse target profiles for each AXL inhibitor with Bemcentinib having the most off-targets, several of which modulate the MAPK pathway. The promiscuity of this drug may explain the Bemcentinib-induced AXL-independent phenotypic and signaling alterations that we and others have observed (58).

AXL has been linked to development of resistance to targeted cancer therapeutics. The mechanistic basis for AXL-mediated drug resistance is yet to be completely elucidated. In this study, we investigated the effect of AXL inhibitors on EGFR TKI resistance in lung cancers using dose-escalation and persister-derived cell line models of Erlotinib resistance. The one common characteristic between all our cell line models of Erlotinib resistance was the overexpression of AXL kinase. Combination treatment with AXL and EGFR TKI failed to re-sensitize the resistant cells to erlotinib in either model of acquired Erlotinib resistance. Several studies have reported that upregulation of AXL in response to EGFR inhibition leads

to resistance to these targeted agents and that genetic and/or pharmaceutical inhibition of AXL restored sensitivity to EGFR inhibitor in these models (7,8,59). However, there are also other groups that have reported that suppression of AXL could not restore the sensitivity of the resistant cells to drug treatment (29,60). These contradictory reports could be attributed to differences in model systems used to study the role of AXL in driving resistance to targeted therapy in cancers. The functional importance of AXL in a particular resistance model can vary depending on the tissue type, driver mutation of the cell line, the method of generation of resistance, and the targeted therapy used. Our data suggests that AXL TKI is unlikely to be an effective strategy in EMT-resistance to EGFR TKI, but other means of targeting AXL, such as antibody-drug conjugates, may be more promising.

Interestingly, despite AXL overexpression in all our Erlotinib-resistant cell line models, we found a unique vulnerability of one persister-derived Erlotinib resistant clone to the combination of Erlotinib and Bemcentinib. This clone, S2–10, is sensitive to the combination of Erlotinib and Bemcentinib, but resistant to both Erlotinib and Bemcentinib as single agents as well as to RXDX106 as a single agent or in combination. This unique AXL-independent phenotypic effect can probably be attributed to the numerous off-targets of Bemcentinib as seen in our ABPP data. The mechanism by which Bemcentinib exerts its AXL-independent phenotypic effects is not fully understood and follow-up studies with functional and phenotypic screens will be needed to answer that question. In PhaseI/II clinical trial combining Bemcentinib with Erlotinib in patients with EGFR-mutant NSCLC, it was reported that 1 of 8 (12.5%) enrolled patients, who had previously progressed on Erlotinib monotherapy, showed a partial response when given Erlotinib and Bemcentinib combination (61). Overall, our data suggests that the promiscuity of Bemcentinib maybe beneficial for its successful transition to clinic, but caution should be exercised if using this drug as tool compound to investigate AXL-driven signaling.

As promising AXL-targeted therapies advance into various stages of clinical trials, a major limitation that needs to be addressed is the development of assays/biomarkers to stratify patients that would most likely benefit from AXL TKI therapy. Since AXL is rarely genetically altered in patients, AXL immunohistochemistry is the most feasible strategy to identify patients. However, immunohistochemistry assays are highly dependent on the quality of the antibody used and have the limitation of providing a measure of protein expression and not protein activity in a sample. For instance, existing studies that have reported AXL expression levels in lung cancers have been highly inconsistent, with expression rates varying from 33–93.2%, probably due to differences in antibodies and evaluation methods used (32). Proximity ligation assays (PLA), that annotate active protein complexes, may be a better and more effective assay for selecting AXL-driven tumors (35). To this end, we have established PLA to detect active AXL:pY signaling complexes in cell line models expressing phosphorylated AXL, which can be developed as an assay to measure drug-targetable active AXL complexes in clinical samples. Interacting proteins and putative substrates identified by BioID and phosphoproteomics respectively, can be used to guide further development of specific proximity ligation assays to detect active AXL signaling complexes as diagnostic tools.

In summary, our study reports a systems level analysis of AXL biology, combining AXL protein complex annotation by BioID, signaling analysis using phosphoproteomics, and characterization of AXL TKI using chemical proteomics to elucidate mechanisms and phenotypes of AXL action.

Supplementary Material

Refer to Web version on PubMed Central for supplementary material.

Acknowledgements

We would like to thank the Gingras lab for providing and helping with the BioID vectors. This work has been supported in part by the Proteomics & Metabolomics, Biostatistics and Bioinformatics, Molecular Genomics, Analytic Microscopy, and Tissue Core Facilities at the H. Lee Moffitt Cancer Center & Research Institute, an NCI designated Comprehensive Cancer Center (P30-CA076292). Funding for this work was supported by National Institutes of Health (5U01CA215709-03) to E.B.H. and A.S.M., and Florida Department of Health Bankhead-Coley program (5BC07) to E.B.H.

References

1. Linger RM, Keating AK, Earp HS, Graham DK. TAM receptor tyrosine kinases: biologic functions, signaling, and potential therapeutic targeting in human cancer. Adv Cancer Res 2008;100:35–83 [PubMed: 18620092]
2. Wu X, Liu X, Koul S, Lee CY, Zhang Z, Halmos B. AXL kinase as a novel target for cancer therapy. Oncotarget 2014;5:9546–63 [PubMed: 25337673]
3. Rankin EB, Giaccia AJ. The Receptor Tyrosine Kinase AXL in Cancer Progression. Cancers (Basel) 2016;8
4. Kim KC, Baek SH, Lee C. Curcumin-induced downregulation of Axl receptor tyrosine kinase inhibits cell proliferation and circumvents chemoresistance in non-small lung cancer cells. Int J Oncol 2015;47:2296–303 [PubMed: 26498137]
5. Aguilera TA, Giaccia AJ. Molecular Pathways: Oncologic Pathways and Their Role in T-cell Exclusion and Immune Evasion-A New Role for the AXL Receptor Tyrosine Kinase. Clin Cancer Res 2017;23:2928–33 [PubMed: 28289089]
6. Asiedu MK, Beauchamp-Perez FD, Ingle JN, Behrens MD, Radisky DC, Knutson KL. AXL induces epithelial-to-mesenchymal transition and regulates the function of breast cancer stem cells. Oncogene 2014;33:1316–24 [PubMed: 23474758]
7. Zhang Z, Lee JC, Lin L, Olivas V, Au V, LaFramboise T, et al. Activation of the AXL kinase causes resistance to EGFR-targeted therapy in lung cancer. Nat Genet 2012;44:852–60 [PubMed: 22751098]
8. Brand TM, Iida M, Stein AP, Corrigan KL, Braverman CM, Luthar N, et al. AXL mediates resistance to cetuximab therapy. Cancer Res 2014;74:5152–64 [PubMed: 25136066]
9. Elkabets M, Pazarentzos E, Juric D, Sheng Q, Pelossof RA, Brook S, et al. AXL mediates resistance to PI3Kalpha inhibition by activating the EGFR/PKC/mTOR axis in head and neck and esophageal squamous cell carcinomas. Cancer Cell 2015;27:533–46 [PubMed: 25873175]
10. Byers LA, Diao L, Wang J, Saintigny P, Girard L, Peyton M, et al. An epithelial-mesenchymal transition gene signature predicts resistance to EGFR and PI3K inhibitors and identifies Axl as a therapeutic target for overcoming EGFR inhibitor resistance. Clin Cancer Res 2013;19:279–90 [PubMed: 23091115]
11. Shieh YS, Lai CY, Kao YR, Shiah SG, Chu YW, Lee HS, et al. Expression of axl in lung adenocarcinoma and correlation with tumor progression. Neoplasia 2005;7:1058–64 [PubMed: 16354588]
12. Ishikawa M, Sonobe M, Nakayama E, Kobayashi M, Kikuchi R, Kitamura J, et al. Higher expression of receptor tyrosine kinase Axl, and differential expression of its ligand, Gas6,

predict poor survival in lung adenocarcinoma patients. Ann Surg Oncol 2013;20 Suppl 3:S467–76 [PubMed: 23242819]

13. Gay CM, Balaji K, Byers LA. Giving AXL the axe: targeting AXL in human malignancy. Br J Cancer 2017;116:415–23 [PubMed: 28072762]
14. Gillette MA, Satpathy S, Cao S, Dhanasekaran SM, Vasaikar SV, Krug K, et al. Proteogenomic Characterization Reveals Therapeutic Vulnerabilities in Lung Adenocarcinoma. Cell 2020;182:200–25 e35 [PubMed: 32649874]
15. Sasaki T, Knyazev PG, Clout NJ, Cheburkin Y, Gohring W, Ullrich A, et al. Structural basis for Gas6-Axl signalling. EMBO J 2006;25:80–7 [PubMed: 16362042]
16. Tanabe K, Nagata K, Ohashi K, Nakano T, Arita H, Mizuno K. Roles of gamma-carboxylation and a sex hormone-binding globulin-like domain in receptor-binding and in biological activities of Gas6. FEBS Lett 1997;408:306–10 [PubMed: 9188782]
17. Lew ED, Oh J, Burrola PG, Lax I, Zagorska A, Traves PG, et al. Differential TAM receptor-ligand-phospholipid interactions delimit differential TAM bioactivities. Elife 2014;3
18. Meyer AS, Zweemer AJ, Lauffenburger DA. The AXL Receptor is a Sensor of Ligand Spatial Heterogeneity. Cell Syst 2015;1:25–36 [PubMed: 26236777]
19. Burchert A, Attar EC, McCloskey P, Fridell YW, Liu ET. Determinants for transformation induced by the Axl receptor tyrosine kinase. Oncogene 1998;16:3177–87 [PubMed: 9671397]
20. Meyer AS, Miller MA, Gertler FB, Lauffenburger DA. The receptor AXL diversifies EGFR signaling and limits the response to EGFR-targeted inhibitors in triple-negative breast cancer cells. Sci Signal 2013;6:ra66
21. Vouri M, Croucher DR, Kennedy SP, An Q, Pilkington GJ, Hafizi S. Axl-EGFR receptor tyrosine kinase hetero-interaction provides EGFR with access to pro-invasive signalling in cancer cells. Oncogenesis 2016;5:e266 [PubMed: 27775700]
22. Kanzaki R, Naito H, Kise K, Takara K, Eino D, Minami M, et al. Gas6 derived from cancer-associated fibroblasts promotes migration of Axl-expressing lung cancer cells during chemotherapy. Sci Rep 2017;7:10613 [PubMed: 28878389]
23. Ben-Batalla I, Schultze A, Wroblewski M, Erdmann R, Heuser M, Waizenegger JS, et al. Axl, a prognostic and therapeutic target in acute myeloid leukemia mediates paracrine crosstalk of leukemia cells with bone marrow stroma. Blood 2013;122:2443–52 [PubMed: 23982172]
24. Mishra A, Wang J, Shiozawa Y, McGee S, Kim J, Jung Y, et al. Hypoxia stabilizes GAS6/Axl signaling in metastatic prostate cancer. Mol Cancer Res 2012;10:703–12 [PubMed: 22516347]
25. Goruppi S, Ruaro E, Schneider C. Gas6, the ligand of Axl tyrosine kinase receptor, has mitogenic and survival activities for serum starved NIH3T3 fibroblasts. Oncogene 1996;12:471–80 [PubMed: 8637702]
26. Shen Y, Chen X, He J, Liao D, Zu X. Axl inhibitors as novel cancer therapeutic agents. Life Sci 2018;198:99–111 [PubMed: 29496493]
27. Zhu C, Wei Y, Wei X. AXL receptor tyrosine kinase as a promising anti-cancer approach: functions, molecular mechanisms and clinical applications. Mol Cancer 2019;18:153 [PubMed: 31684958]
28. Bansal N, Mishra PJ, Stein M, DiPaola RS, Bertino JR. Axl receptor tyrosine kinase is up-regulated in metformin resistant prostate cancer cells. Oncotarget 2015;6:15321–31 [PubMed: 26036314]
29. Wilson C, Ye X, Pham T, Lin E, Chan S, McNamara E, et al. AXL inhibition sensitizes mesenchymal cancer cells to antimitotic drugs. Cancer Res 2014;74:5878–90 [PubMed: 25125659]
30. Sharifnia T, Rusu V, Piccioni F, Bagul M, Imielinski M, Cherniack AD, et al. Genetic modifiers of EGFR dependence in non-small cell lung cancer. Proc Natl Acad Sci U S A 2014;111:18661–6 [PubMed: 25512530]
31. Antony J, Huang RY. AXL-Driven EMT State as a Targetable Conduit in Cancer. Cancer Res 2017;77:3725–32 [PubMed: 28667075]
32. Zhang G, Wang M, Zhao H, Cui W. Function of Axl receptor tyrosine kinase in non-small cell lung cancer. Oncol Lett 2018;15:2726–34 [PubMed: 29434997]

33. Samavarchi-Tehrani P, Abdouni H, Samson R, Gingras AC. A Versatile Lentiviral Delivery Toolkit for Proximity-dependent Biotinylation in Diverse Cell Types. Mol Cell Proteomics 2018;17:2256–69 [PubMed: 29991506]
34. Kuenzi BM, Borne AL, Li J, Haura EB, Eschrich SA, Koomen JM, et al. APOSTL: An Interactive Galaxy Pipeline for Reproducible Analysis of Affinity Proteomics Data. J Proteome Res 2016;15:4747–54 [PubMed: 27680298]
35. Smith MA, Hall R, Fisher K, Haake SM, Khalil F, Schabath MB, et al. Annotation of human cancers with EGFR signaling-associated protein complexes using proximity ligation assays. Sci Signal 2015;8:ra4
36. Tyanova S, Temu T, Cox J. The MaxQuant computational platform for mass spectrometry-based shotgun proteomics. Nat Protoc 2016;11:2301–19 [PubMed: 27809316]
37. Yoshida T, Song L, Bai Y, Kinose F, Li J, Ohaegbulam KC, et al. ZEB1 Mediates Acquired Resistance to the Epidermal Growth Factor Receptor-Tyrosine Kinase Inhibitors in Non-Small Cell Lung Cancer. PLoS One 2016;11:e0147344
38. Ramirez M, Rajaram S, Steininger RJ, Osipchuk D, Roth MA, Morinishi LS, et al. Diverse drug-resistance mechanisms can emerge from drug-tolerant cancer persister cells. Nat Commun 2016;7:10690 [PubMed: 26891683]
39. Love MI, Huber W, Anders S. Moderated estimation of fold change and dispersion for RNA-seq data with DESeq2. Genome Biol 2014;15:550 [PubMed: 25516281]
40. Subramanian A, Tamayo P, Mootha VK, Mukherjee S, Ebert BL, Gillette MA, et al. Gene set enrichment analysis: a knowledge-based approach for interpreting genome-wide expression profiles. Proc Natl Acad Sci U S A 2005;102:15545–50 [PubMed: 16199517]
41. Gu Z, Eils R, Schlesner M. Complex heatmaps reveal patterns and correlations in multidimensional genomic data. Bioinformatics 2016;32:2847–9 [PubMed: 27207943]
42. Kim JE, Kim Y, Li G, Kim ST, Kim K, Park SH, et al. MerTK inhibition by RXDX-106 in MerTK activated gastric cancer cell lines. Oncotarget 2017;8:105727–34
43. Xue Y, Ren J, Gao X, Jin C, Wen L, Yao X. GPS 2.0, a tool to predict kinase-specific phosphorylation sites in hierarchy. Mol Cell Proteomics 2008;7:1598–608 [PubMed: 18463090]
44. Yang PW, Liu YC, Chang YH, Lin CC, Huang PM, Hua KT, et al. Cabozantinib (XL184) and R428 (BGB324) Inhibit the Growth of Esophageal Squamous Cell Carcinoma (ESCC). Front Oncol 2019;9:1138 [PubMed: 31781483]
45. Palve V, Liao Y, Remsing Rix LL, Rix U. Turning liabilities into opportunities: Off-target based drug repurposing in cancer. Semin Cancer Biol 2020
46. Grullich C. Cabozantinib: Multi-kinase Inhibitor of MET, AXL, RET, and VEGFR2. Recent Results Cancer Res 2018;211:67–75 [PubMed: 30069760]
47. Holland SJ, Pan A, Franci C, Hu Y, Chang B, Li W, et al. R428, a selective small molecule inhibitor of Axl kinase, blocks tumor spread and prolongs survival in models of metastatic breast cancer. Cancer Res 2010;70:1544–54 [PubMed: 20145120]
48. Okerberg ES, Wu J, Zhang B, Samii B, Blackford K, Winn DT, et al. High-resolution functional proteomics by active-site peptide profiling. Proc Natl Acad Sci U S A 2005;102:4996–5001 [PubMed: 15795380]
49. Cravatt BF, Wright AT, Kozarich JW. Activity-based protein profiling: from enzyme chemistry to proteomic chemistry. Annu Rev Biochem 2008;77:383–414 [PubMed: 18366325]
50. Chen EY, Tan CM, Kou Y, Duan Q, Wang Z, Meirelles GV, et al. Enrichr: interactive and collaborative HTML5 gene list enrichment analysis tool. BMC Bioinformatics 2013;14:128 [PubMed: 23586463]
51. Qu XH, Liu JL, Zhong XW, Li XI, Zhang QG. Insights into the roles of hnRNP A2/B1 and AXL in non-small cell lung cancer. Oncol Lett 2015;10:1677–85 [PubMed: 26622731]
52. Solanki HS, Welsh EA, Fang B, Izumi V, Darville L, Stone B, et al. Cell Type-specific Adaptive Signaling Responses to KRAS(G12C) Inhibition. Clin Cancer Res 2021;27:2533–48 [PubMed: 33619172]
53. Lay JD, Hong CC, Huang JS, Yang YY, Pao CY, Liu CH, et al. Sulfasalazine suppresses drug resistance and invasiveness of lung adenocarcinoma cells expressing AXL. Cancer Res 2007;67:3878–87 [PubMed: 17440102]

54. Mudduluru G, Vajkoczy P, Allgayer H. Myeloid zinc finger 1 induces migration, invasion, and in vivo metastasis through Axl gene expression in solid cancer. Mol Cancer Res 2010;8:159–69 [PubMed: 20145042]

55. Hafizi S, Dahlback B. Signalling and functional diversity within the Axl subfamily of receptor tyrosine kinases. Cytokine Growth Factor Rev 2006;17:295–304 [PubMed: 16737840]

56. Fridell YW, Jin Y, Quilliam LA, Burchert A, McCloskey P, Spizz G, et al. Differential activation of the Ras/extracellular-signal-regulated protein kinase pathway is responsible for the biological consequences induced by the Axl receptor tyrosine kinase. Mol Cell Biol 1996;16:135–45 [PubMed: 8524290]

57. Braunger J, Schleithoff L, Schulz AS, Kessler H, Lammers R, Ullrich A, et al. Intracellular signaling of the Ufo/Axl receptor tyrosine kinase is mediated mainly by a multi-substrate docking-site. Oncogene 1997;14:2619–31 [PubMed: 9178760]

58. Chen F, Song Q, Yu Q. Axl inhibitor R428 induces apoptosis of cancer cells by blocking lysosomal acidification and recycling independent of Axl inhibition. Am J Cancer Res 2018;8:1466–82 [PubMed: 30210917]

59. Giles KM, Kalinowski FC, Candy PA, Epis MR, Zhang PM, Redfern AD, et al. Axl mediates acquired resistance of head and neck cancer cells to the epidermal growth factor receptor inhibitor erlotinib. Mol Cancer Ther 2013;12:2541–58 [PubMed: 24026012]

60. Suda K, Mizuuchi H, Sato K, Takemoto T, Iwasaki T, Mitsudomi T. The insulin-like growth factor 1 receptor causes acquired resistance to erlotinib in lung cancer cells with the wild-type epidermal growth factor receptor. Int J Cancer 2014;135:1002–6 [PubMed: 24458568]

61. Byers L, Gold K, Peguero J, Johnson M, Nieva J, Harb W, et al. P2.13–10 Ph I/II Study of Oral Selective AXL Inhibitor Bemcentinib (BGB324) in Combination with Erlotinib in pts with EGFRm NSCLC. Journal of Thoracic Oncology 2018;13:S801–S2

62. Perez-Riverol Y, Csordas A, Bai J, Bernal-Llinares M, Hewapathirana S, Kundu DJ, et al. The PRIDE database and related tools and resources in 2019: improving support for quantification data. Nucleic Acids Res 2019;47:D442–D50 [PubMed: 30395289]

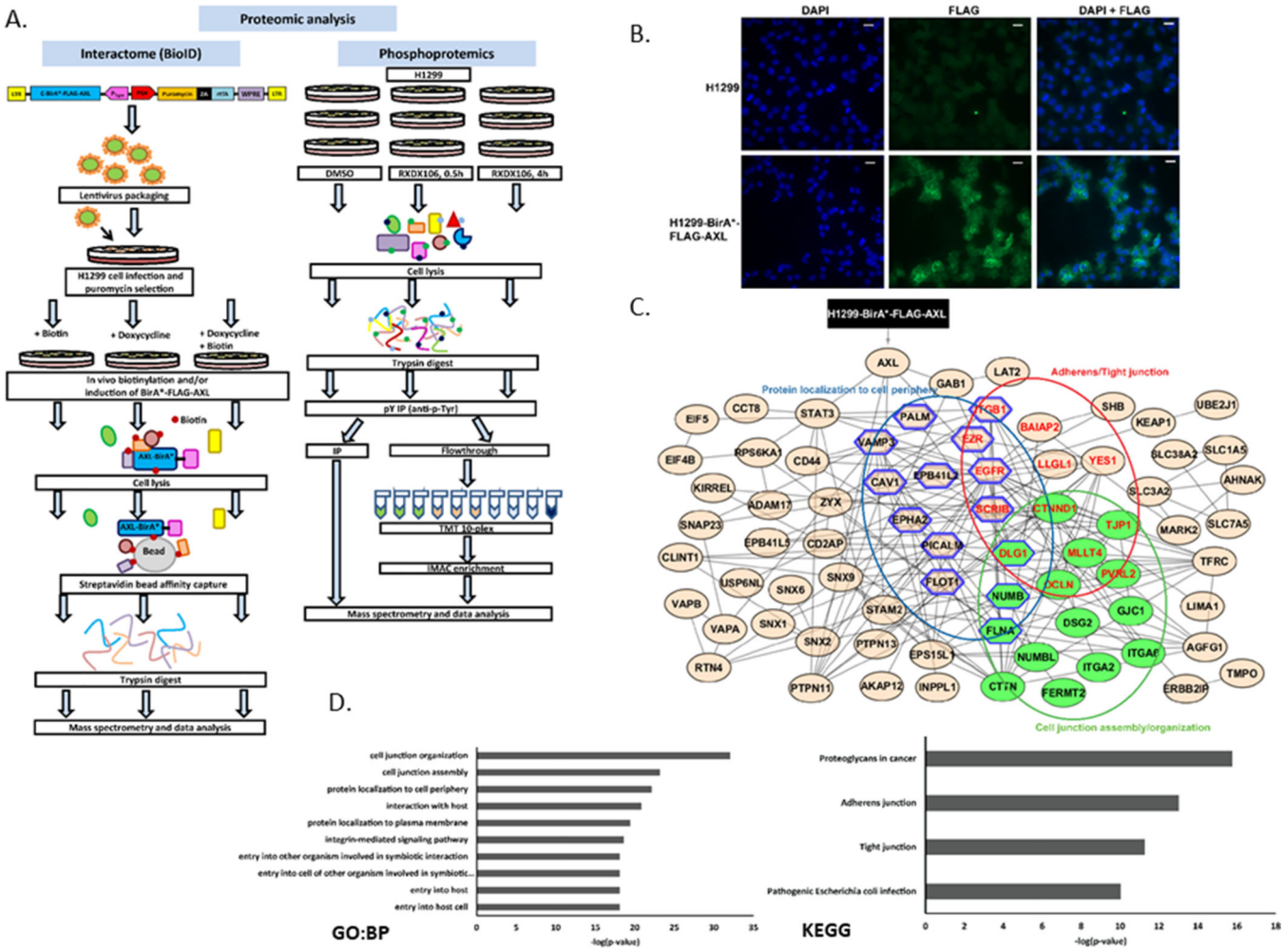

Figure 1. Proteomic characterization of the AXL interactome.

(A) Schematic of the workflow integrating multiple proteomics approaches (BioID, tyrosine and global phosphoproteomics). (B) Immunofluorescence staining showing expression of FLAG in H1299 cells with or without the pSTV6-BirA*-FLAG-AXL transgene. Images were acquired at 20X. DAPI nuclear stain: blue; FLAG: green. (C) STRING network of AXL interacting proteins as identified via BioID pulldowns followed by APOSTL analysis. Only connected nodes are shown. Nodes are grouped and colored in Cytoscape as per the enrichment analysis shown in (D). Green nodes: cell junction assembly/organization; blue hexagon: protein localization to cell periphery; red labels: Adherens/tight junction. (D) Gene Ontology (GO)- Biological Process (BP) and KEGG enrichment analyses of AXL interactome using APOSTL.

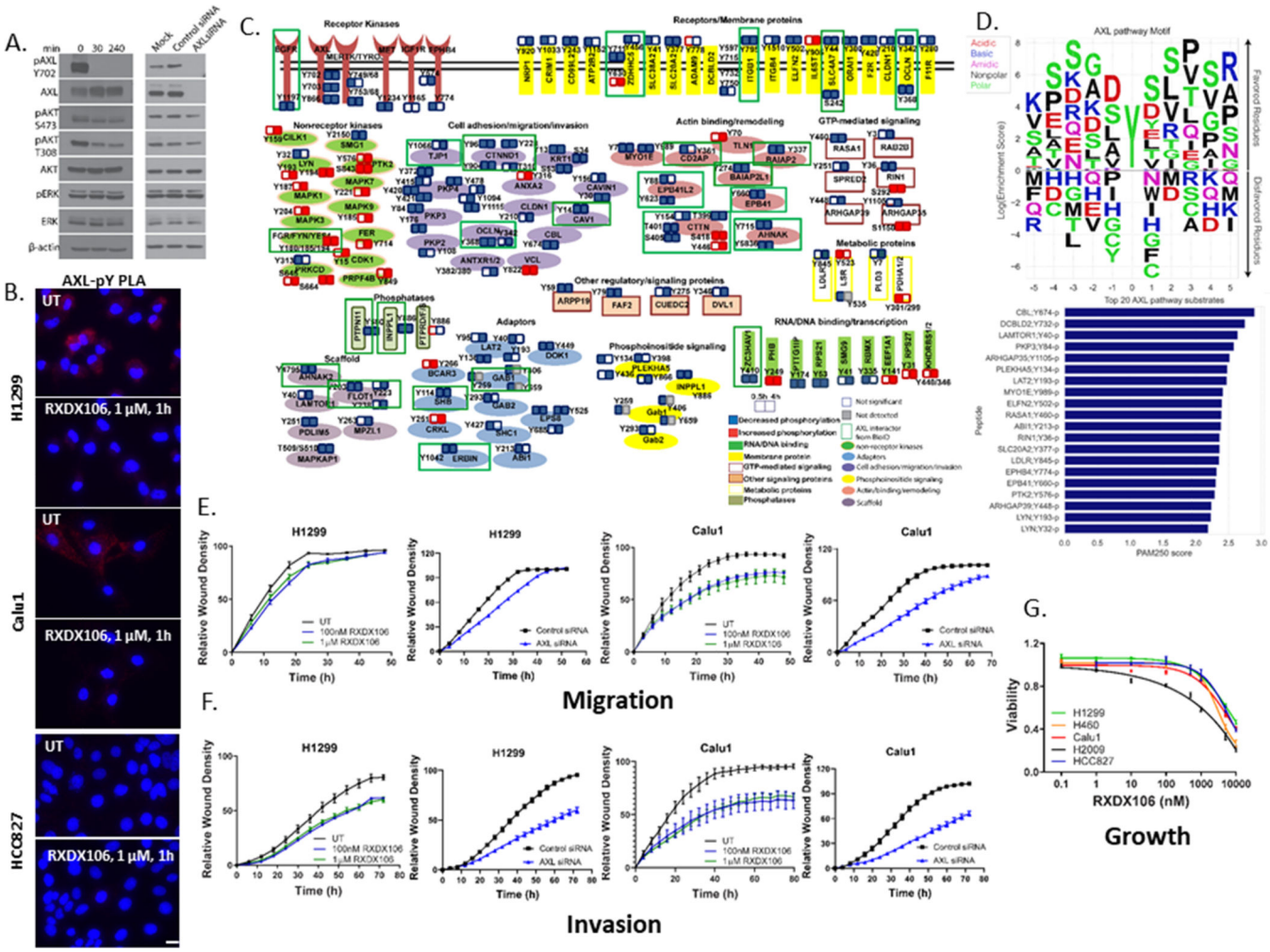

Figure 2. Phosphoproteome responses to AXL inhibition by RXDX106 in H1299 lung cancer cells.

(A) Immunoblot analysis of downstream signaling in H1299 after treatment either with 100 nM RXDX106 for the indicated times or AXL siRNA for 48h. Shown is a representative of three replicate experiments (B) Proximity ligation assay for AXL-pY complexes in the indicated cell lines with or without exposure to 1 μM RXDX106 for 1h. Images were acquired at 40X magnification. Shown is a representative of two replicate experiments (C) Overview of proteins modulated by tyrosine phosphorylation after RXDX106 exposure, grouped according to their cellular function. Each functional group is represented by a different color/shape as shown in the legend (D) Peptide sequences of proteins from the pY dataset that overlapped with the BioID data were used to build a Position-Specific-Scoring-Matrix (PSSM) AXL pathway substrate motif. Also shown are the top 20 putative AXL pathway substrates as a function of their mean PAM250 similarity scores (E-F) Scratch wound migration (E) and invasion (F) assays where relative wound density of H1299 and Calu1 cells, treated either with RXDX106 or AXL siRNA, were analyzed on the IncuCyte every 3h until the scratch wound is healed (~48 – 72h). Data is represented as mean ± SE and is representative of three replicate experiments (G) Relative viability of NSCLC cell lines expressing varying levels of phosphorylated and total AXL as assessed by

CellTiter-Glo after 72 h of treatment with increasing concentrations of RXDX-106. Data are represented as mean ± SE and is the average of three replicate experiments.

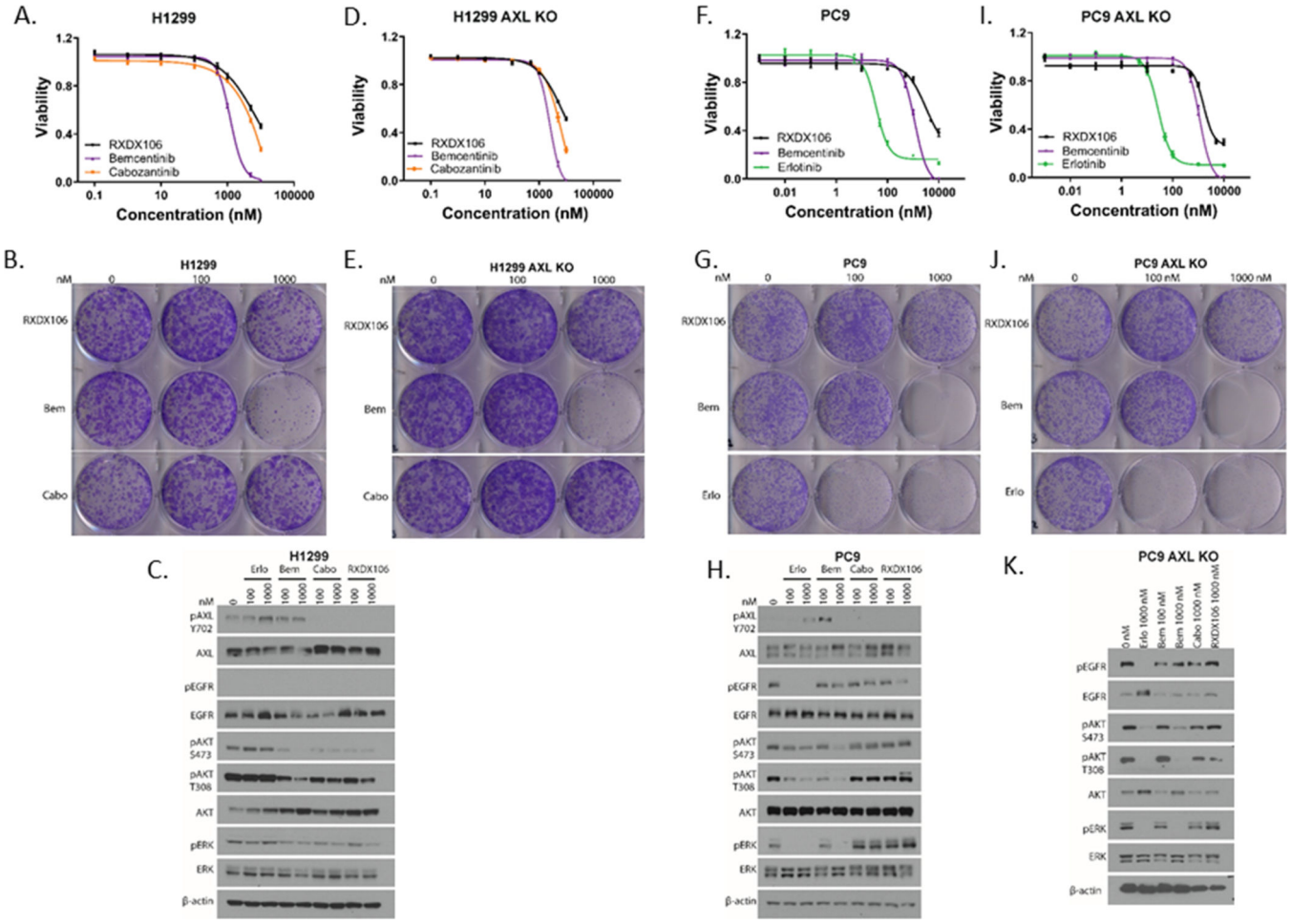

Figure 3. Differential phenotypic effects of AXL inhibitors on NSCLC cell lines.

Relative viability of H1299 (A), H1299 AXL KO (D), PC9 (F), and PC9 AXL KO (I) cells upon 72h treatment with increasing concentrations of the indicated drugs as measured by CellTiterGlo. Data are represented as mean ± SE and is the average of two independent experiments. Colony formation assay of H1299 (B), H1299 AXL KO (E), PC9 (G), and PC9 AXL KO (J) cells post treatment with the indicated doses of RXDX-106, Bemcentinib (Bem), Cabozantinib (Cabo) or Erlotinib (Erlo) for 9 days. Immunoblot analyses showing alterations in downstream signaling in H1299 (C), PC9 (H), and PC9 AXL KO (K) cells when exposed to the indicated concentrations of the different drugs for 1h. Shown is representative of three independent experiments.

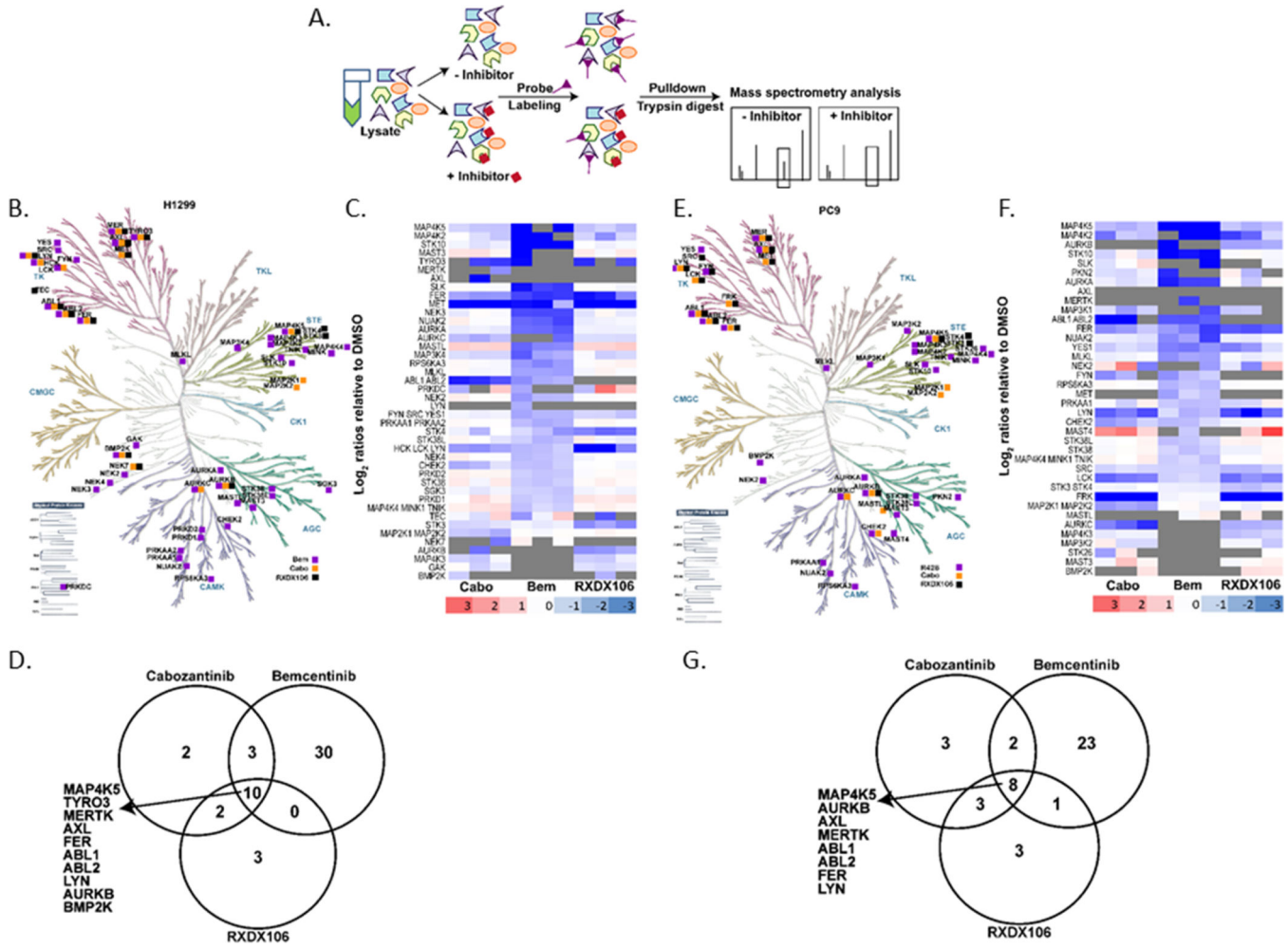

Figure 4. Activity-based protein profiling (ABPP) reveals differential targets of AXL inhibitors.
(A) Schematic representation of ABPP workflow. Kinome trees showing comparative kinase binding profiles of RXDX106, Bemcentinib, and Cabozantinib in H1299 (B) and PC9 (E) cells. Kinome phylogenetic tree adapted courtesy of Cell Signaling Technology. Heatmap representation of $\log_2$ ratios relative to DMSO for selected kinase targets for each drug in H1299 (C) and PC9 (F) cells. Venn diagrams representing number of kinase targets for each AXL TKI in H1299 (D) and PC9 (G) cells. Kinases that are common targets for all 3 drugs in each cell linse have been listed.

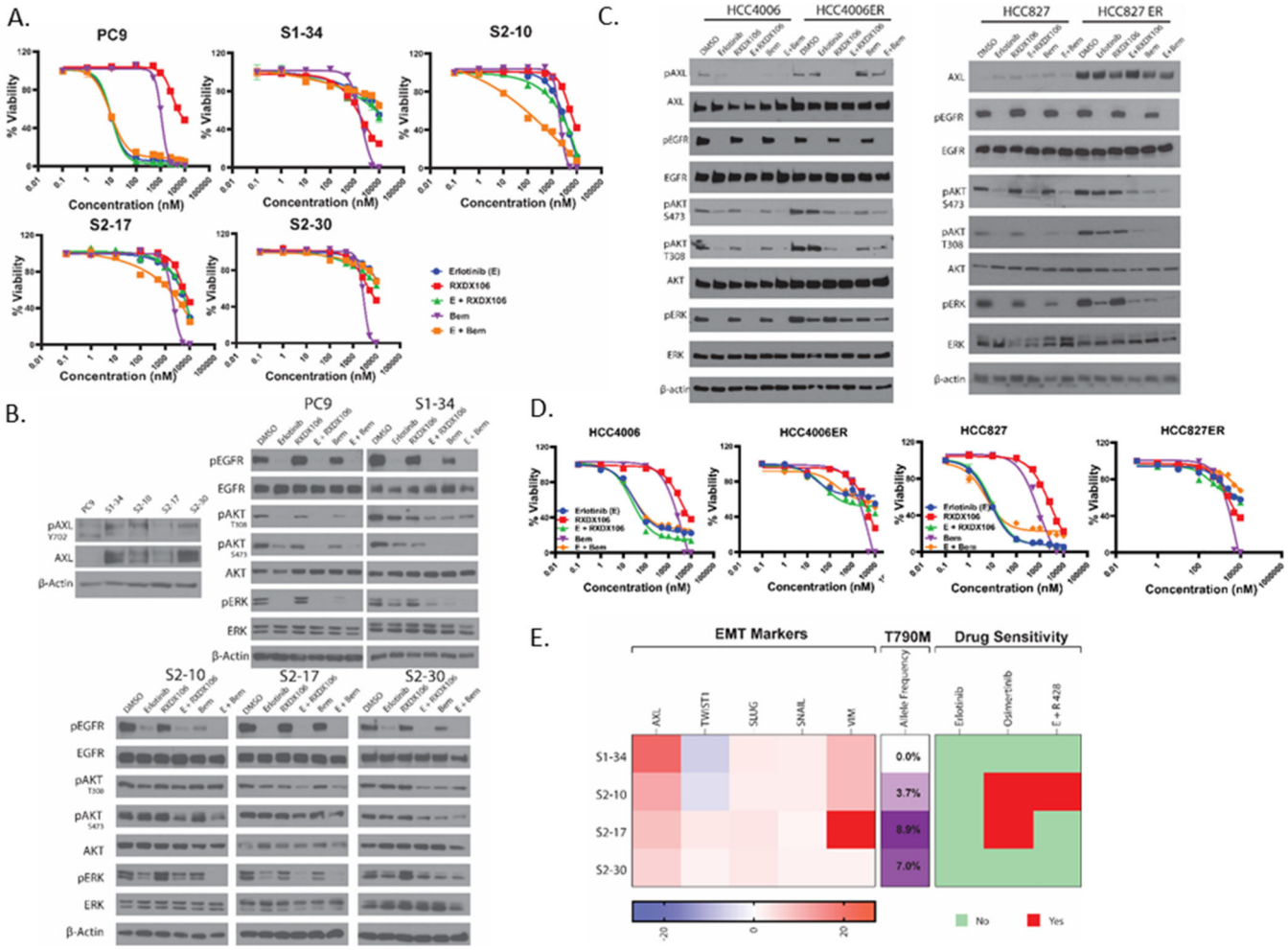

Figure 5. Effect of AXL inhibition on cell line models of erlotinib-resistance.

(A) Relative viability of PC9 and persister-derived erlotinib-resistant cells, as measured by CellTiter Glo after 72h treatment with increasing doses of the indicated drugs. For the AXL and EGFR TKI combination treatment, 1 μM of AXL inhibitor was used with increasing doses of erlotinib treatment. Data are represented as mean ± SE. (B) Immunoblot analysis of AXL expression and phosphorylation as well as alterations in downstream signaling proteins in PC9 and persister-derived erlotinib-resistant cells with or without treatment with 1μM of the indicated drugs for 1h. (C) Immunoblot assay showing changes in downstream signaling proteins in HCC4006 and HCC827 cells and their erlotinib-resistant derivative cells HCC4006ER and HCC827ER, upon treatment with 1μM of the indicated drugs for 1h. (D) Relative viability of HCC4006 and HCC827 parental and ER cells as measured by CellTiter Glo after 72h treatment with increasing doses of the indicated drugs. For the AXL and EGFR TKI combination treatment, 1 μM of AXL inhibitor was used with increasing doses of erlotinib treatment. Data are represented as mean ± SE. (E) Characterization of the persister-derived resistant clones is summarized here, highlighting differences in RNA expression of various EMT markers, allele frequencies of the T790M “gatekeeper” mutation, and sensitivity to different EGFR and AXL TKIs. All data shown are representative of three independent experiments.

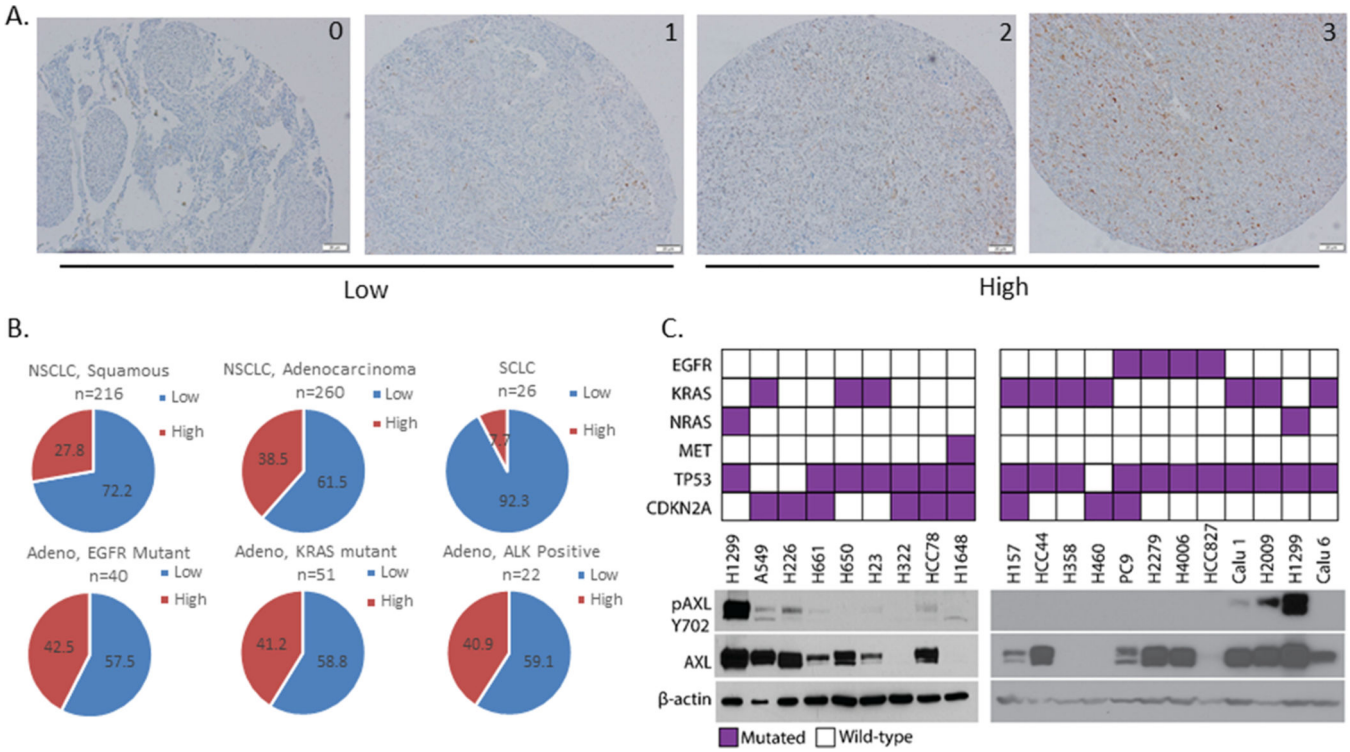

Figure 6. AXL expression in patient tumor specimens and cell lines in lung cancer.

AXL IHC was performed on patient tumor specimens. Staining intensity was graded as 0=none, 1=weak, 2= moderate, and 3=strong. (A) Representative images for each scoring grade, acquired at 20X. (B) Graphs showing distribution of AXL expression in tumor samples of the indicated types. IHC scores were grouped as low (0 or 1) or high (2 or 3). *n* indicates the number of specimens of the indicated type used for analysis. (C) Immunoblot analysis showing phosphoTyr^{702}- and total AXL protein levels in a panel of NSCLC cell lines. The driver mutation for each cell line is indicated in the top panel. β-actin protein levels were used as a loading control.